



HAL
open science

An independent, landmark-dominated head-direction signal in dysgranular retrosplenial cortex

Pierre-Yves Jacob, Giulio Casali, Laure Spieser, Hector Page, Dorothy Overington, Kate Jeffery

► To cite this version:

Pierre-Yves Jacob, Giulio Casali, Laure Spieser, Hector Page, Dorothy Overington, et al.. An independent, landmark-dominated head-direction signal in dysgranular retrosplenial cortex. *Nature Neuroscience*, 2016, 20 (2), pp.173-175. 10.1038/nn.4465 . hal-01664366v1

HAL Id: hal-01664366

<https://hal.science/hal-01664366v1>

Submitted on 15 Dec 2017 (v1), last revised 8 Jan 2018 (v2)

HAL is a multi-disciplinary open access archive for the deposit and dissemination of scientific research documents, whether they are published or not. The documents may come from teaching and research institutions in France or abroad, or from public or private research centers.

L'archive ouverte pluridisciplinaire **HAL**, est destinée au dépôt et à la diffusion de documents scientifiques de niveau recherche, publiés ou non, émanant des établissements d'enseignement et de recherche français ou étrangers, des laboratoires publics ou privés.

1 **An independent, landmark-dominated head direction**

2 **signal in dysgranular retrosplenial cortex**

3 **Author list and affiliations**

4 Pierre-Yves Jacob^{1*}, Giulio Casali¹, Laure Spieser², Hector Page¹, Dorothy Overington¹, Kate
5 Jeffery^{1*}

6 ¹ Institute of Behavioural Neuroscience, Research Department of Experimental Psychology,
7 Division of Psychology and Language Sciences, University College London, London, UK.

8 ² Department of Psychology, City University of London, London, UK.

9 Correspondence to: Kate Jeffery (k.jeffery@ucl.ac.uk)

10 **Abstract**

11 We investigated how landmarks influence the brain's computation of head direction and
12 found that in a bi-directionally symmetrical environment, some neurons in dysgranular
13 retrosplenial cortex showed bi-directional firing patterns. This indicates dominance of neural
14 activity by local environmental cues even when these conflict with the global head direction
15 signal. It suggests a mechanism for associating landmarks to or dissociating them from the
16 head direction signal, according to their directional stability/utility.

17 **Main text**

18 The "sense of direction" is computed by head direction (HD) cells¹, which fire when the
19 animal faces a particular direction. The head direction signal is derived from learned

20 environmental landmarks², but the brain needs to know that these are spatially stable before it
21 can use them as directional markers³. This circular problem thus requires an interplay
22 between the existing directional representation and newly encountered landmarks. We
23 investigated the hypothesis that retrosplenial cortex (RSC), a HD structure that processes
24 landmark stability⁴, is involved in this interplay process. RSC is a cortical region⁵⁻⁷ that is
25 directly connected to visual cortex as well as to the main HD network⁸. We exposed rats to an
26 environment where global and local directional cues were in conflict and recorded RSC
27 neurons, as well as head direction cells from anterior thalamus and post-subiculum. Rats
28 freely moved between two connected, rectangular compartments (**Supplementary Fig. 1**),
29 each having landmarks that were reversed in orientation relative to those in the other, thus
30 dissociating local landmarks and global direction. To orient the global head direction system,
31 the symmetry of the apparatus was broken by scenting one compartment with lemon and the
32 other with vanilla.

33 Of 1090 RSC neurons (**Supplementary Table 1**), we identified 96 classic HD cells (9%),
34 each with a single tuning curve that maintained a constant direction across compartments and
35 thus reversed its relation to the local cues depending on odor context (**Fig. 1a**,
36 **Supplementary Fig. 2** and **Supplementary Table 2**). This confirms that HD cells can use
37 odor-context information to resolve spatial ambiguity. However, many neurons had two
38 opposing head-direction tuning curves (**Fig. 1b**; **Supplementary Fig. 3**). We derived a
39 measure of this bi-directional firing to identify 116 of these ‘bi-directional’ (BD) cells (11%)
40 (**Supplementary Fig. 4**) and undertook several analyses to rule out that the bi-directional
41 pattern could have been recording artefact (**Supplementary Fig. 5**). Moreover, many BD
42 cells showed compartment-specific activity (see below), meaning that the individuals in the
43 putative cell-pairs would have to have fired in only one compartment, which has never been
44 observed in HD cells.

45 Forty-six of the BD neurons were compartment-specific (**Fig. 1b and Supplementary Fig.**
46 **3**), meaning that the cells actually had uni-directional firing but this reversed each time the rat
47 passed through the doorway, producing a bi-directional pattern overall. This was shown by
48 analyzing each compartment separately and also by closing the door, after which tuning
49 curves became uni-directional (**Fig. 1b**). This reversal between compartments means that the
50 tuning curves maintained the same relationship to the local landmarks. BD cells were
51 recorded simultaneously with the non-reversing HD cells (**Fig. 1c; Supplementary Fig. 6**),
52 such that the cells dissociated their responses when the rat changed compartments. BD cells
53 also followed apparatus rotation more reliably than HD cells (**Supplementary Fig. 7**). Thus,
54 a population of RSC neurons is dissociable from the main head direction network and is
55 dominated by landmarks, an observation that refutes the previous belief that the entire head
56 direction network is coherent^{9,10}.

57 We looked for bi-directional firing in two other HD-cell regions, postsubiculum and the
58 anterior thalamus, but here found only classic HD cells (**Fig. 2a**). In addition, histology
59 revealed that BD cells were recorded exclusively in the dysgranular RSC, while HD cells
60 were distributed across both granular and dysgranular RSC (**Fig 2b; Supplementary Fig. 8**).

61 To test whether the bi-directional pattern is dependent on the rotated local visual cues, we
62 recorded 12 BD cells in darkness: they maintained their bi-directional pattern
63 (**Supplementary Fig. 9a-c**), suggesting that multimodal inputs can support the directionality
64 of firing. Interestingly, 9 BD cells recorded in an open field lost their bi-directional pattern
65 (**Supplementary Fig. 9d, e**).

66 Unexpectedly, as well as the 46 cells described above that reversed firing between
67 compartments, which we named between-compartment bi-directional cells (BC-BD), we

68 found 70 cells that expressed a bi-directional pattern *within* each compartment (**Fig. 2c and**
69 **Fig. 3a, b; Supplementary Fig. 10**). As before, detailed analyses ruled out that the within-
70 compartment bi-directional (WC-BD) cells could have been recording artefact. The doubled
71 tuning curves were slightly asymmetric, with a dominant (slightly larger) peak that reversed
72 direction between compartments (**Fig. 3c**), indicating a contributing influence of local
73 landmarks. We examined whether WC-BD cells expressed two simultaneous tuning curves,
74 or a single curve that reversed frequently within compartments. Two tuning curves might
75 result in increased overall spike count relative to HD cells (because the cells can fire in two
76 directions instead of just one), while a single tuning curve that switched would result in lower
77 and more variable firing rates and a higher proportion of pauses in firing, producing long
78 inter-spike intervals (ISIs). In fact, spike count was intermediate, being 37% higher than for
79 HD cells, and 42% higher than for BC-BD cells, both differences being significant (**Fig 3d**).
80 Firing rates did not differ for the three directional cell types, either for peak rates or mean
81 rates (**Supplementary Table 3**). Also, spread of firing rates was no different (Fig 3e), and
82 inter-spike interval (ISI) analysis showed no increase in long intervals; moreover, analysis of
83 the ISI histogram decay time-to-half-peak showed no difference between cell types
84 (**Supplementary Table 3**). Taken together, these results suggest that WC-BD cells have true
85 dual tuning curves, one being slightly smaller, rather than single, periodically reversing ones.

86 What could cause this within-compartment bi-directional pattern? It is likely due to the rat's
87 previous experience of the two-compartment space and may reflect acquisition of new inputs
88 from co-active HD cells during initial exploration (**Supplementary Fig. 11**). In our
89 apparatus, because of the visual reversal, a landmark-driven BD cell is co-active with two
90 sets of HD cells having opposing firing directions. If these HD cells become additional new
91 inputs due to Hebbian learning, the cell would now be driven to fire in both directions. This
92 could explain why for WC-BD cells, one tuning curve was slightly stronger (because it has

93 additional drive from the landmarks), and why this asymmetry was compartment-specific
94 (**Fig. 3c**). As well as evidence of interaction with the head direction signal, we found
95 evidence of spatially modulated activity in a subset of cells (**Supplementary Fig. 12**),
96 suggesting a more general integrative role for this region.

97 What could be the function of BD cells? It may be to mediate both ways between visual
98 landmarks and the global HD signal. A network of neurons having varying degrees of
99 coupling between the two systems could use landmarks to compute head direction and, at the
100 same time, use the head direction signal to compute landmark stability; in this
101 “bootstrapping” manner, stable landmarks could be added to the constellation of inputs able
102 to drive head direction cells, and unstable landmarks removed from it. This hypothesis is
103 consistent with evidence from gene activation studies suggesting a role for dysgranular RSC
104 in spatial tasks requiring light (i.e. vision) but not darkness^{11,12}, human neuroimaging studies
105 showing a role for RSC in monitoring landmark stability⁴ and local reference frames¹³, or
106 integrating across scenes¹⁴, and from recording studies suggesting plasticity in the
107 connections of landmarks to the HD network¹⁵. Thus, the network could function to learn
108 which cues are the directionally stable ones that have a consistent relationship to the head
109 direction signal, and so can act as landmarks to define a local directional reference frame.

110 **Acknowledgments**

111 This work was supported by grants from the Medical Research Council (G1100669) and
112 Wellcome Trust (103896AIA) to K.J.

113 **Author contributions**

114 K.J. conceived the study and obtained funding, P.Y.J. and K.J. designed the protocol, P.Y.J.
115 and D.O. performed surgeries and recordings, P.Y.J., L.S., G.C. and H.P. analysed data. All
116 authors interpreted data and discussed results. P.Y.J. and K.J. wrote the manuscript. All
117 authors commented and edited the manuscript.

118 **Competing financial interests**

119 KJ is a non-shareholding director of Axona Ltd

120 **References and notes**

- 121 1. Taube, J.S. *Annu. Rev. Neurosci.* **30**, 181–207 (2007).
- 122 2. Taube, J.S. & Burton, H.L. *J. Neurophysiol.* **74**, 1953–1971 (1995).
- 123 3. Knierim, J.J., Kudrimoti, H.S. & McNaughton, B.L. *J. Neurosci.* **15**, 1648–1659
124 (1995).
- 125 4. Auger, S.D., Mullally, S.L. & Maguire, E.A. *PLoS One* **7**, e43620 (2012).
- 126 5. Chen, L.L., Lin, L.H., Green, E.J., Barnes, C.A. & McNaughton, B.L. *Exp. Brain Res.*
127 **101**, 8–23 (1994).
- 128 6. Chen, L.L., Lin, L.H., Barnes, C.A. & McNaughton, B.L. *Exp. Brain Res.* **101**, 24–34
129 (1994).
- 130 7. Cho, J. & Sharp, P.E. *Behav Neurosci* **115**, 3–25 (2001).

- 131 8. Sugar, J., Witter, M.P., van Strien, N.M. & Cappaert, N.L.M. *Front. Neuroinform.* **5**, 7
132 (2011).
- 133 9. Taube, J.S., Muller, R.U. & Ranck-JB, J. *J. Neurosci.* **10**, 436–447 (1990).
- 134 10. Yoganarasimha, D. *J. Neurosci.* **26**, 622–631 (2006).
- 135 11. Cooper, B.G., Manka, T.F. & Mizumori, S.J. *Behav Neurosci* **115**, 1012–1028 (2001).
- 136 12. Pothuizen, H.H.J., Davies, M., Albasser, M.M., Aggleton, J.P. & Vann, S.D. *Eur. J.*
137 *Neurosci.* **30**, 877–888 (2009).
- 138 13. Marchette, S.A., Vass, L.K., Ryan, J. & Epstein, R.A. *Nat. Neurosci.* **17**, 1598–1606
139 (2014).
- 140 14. Robertson, C.E., Hermann, K.L., Mynick, A., Kravitz, D.J. & Kanwisher, N. *Curr.*
141 *Biol.* **26**, 2463–2468 (2016).
- 142 15. Knight, R. et al. *Philos. Trans. R. Soc. Lond. B. Biol. Sci.* **369**, 20120512 (2014).
- 143 16. Kadir, S.N., Goodman, D.F.M. & Harris, K.D. *Neural Comput.* **26**, 2379–94 (2014).
- 144 17. Bonnevie, T. et al. *Nat. Neurosci.* **16**, 309–17 (2013).
- 145 18. Giocomo, L.M. et al. *Curr. Biol.* **24**, 252–262 (2014).
- 146 19. Paxinos, G. & Watson, C. *Elsevier Acad. Press* **170**, 547–612 (2007).

147 **Figure legends**

148 **Figure 1: Two types of directional encoding by RSC neurons. a,** Example of an RSC HD
149 cell. Top: Orientation of the apparatus (cross-hatching = unavailable). Bottom: polar plots of
150 firing rate vs. head direction (no. = peak rate). **b,** Example of an RSC bi-directional (BD) cell.
151 Tuning curves (third row) are color-coded according to the color key (second row). Fourth
152 row: directional color-coding of action potentials, superimposed on the animal's path (grey),
153 reveals the compartment-specificity of firing directions. Bottom row: tuning curves from each
154 sub-compartment in isolation. **c,** Simultaneous recordings of a BD cell and a classic (uni-
155 directional) HD cell, color-coded as before, revealing the dissociation in tuning curve
156 direction.

157 **Figure 2: Bi-directional cells are specific to dysgranular RSC. a,** Distribution of bi-
158 directional firing patterns ("flip score") as a function of directional tuning (calculated as
159 angle-doubled Rayleigh vector length – see Methods) for 1090 RSC cells, and postsubiculum
160 (PoS) and anterior thalamus (ADN) cells in trial 1. Gray lines show the Rayleigh vector and
161 flip score thresholds for determining all directional cells and BD cells, respectively. Top,
162 scatter plot showing BD cells (orange) and HD cells (green). Bottom, density plots of the
163 same data revealing two clear populations. **b,** Recording sites of BD (orange) and HD (green)
164 cells within the dysgranular (dRSC, dark gray) and granular (gRSC, light gray) RSC.
165 **c,** Density plots of RSC BD cells across 5 recording trials, collapsed across cells/sessions.
166 Note that some cells became uni-directional (low flip score) when the door closed.

167 **Figure 3: Within-compartmental bi-directional activity. a,** Example of a within-
168 compartment bi-directional (WC-BD) cell. **b,** 70/116 (60%) showed within-compartmental
169 bi-directionality. **c,** Size asymmetry of tuning curves in the WC-BD cells is compartment-

170 specific. Direction 1 was defined as the direction of the biggest peak in the lemon
171 compartment, and direction 2 the opposite. Overall, firing rates were similar in the two
172 compartments (left), but the direction of the dominant peak reversed between compartments.
173 **d,e** Analysis of spike count (d) revealed an increase in spiking for WC-BD cells (1557.49 +/-
174 41.86) compared with the BC-BD cells (1058.93 +/- 128.75) and the HD cells (1041.26 +/-
175 117.65; one-way ANOVA, [F(2,209) = 5.00, p = 0.01]; * = p < 0.05). However, firing rate
176 spread, measured as the standard deviation (SD) of firing rates (e) was not different between
177 cell types, being 3.80 +/- 0.23 for HD cells, 4.90 +/- 0.49 for BC-BD cells and 4.41 +/- 0.33
178 for WC-BD cells [F(2,209) = 2.80, p = 0.07]. Solid lines show mean and s.e.m.

179 **Methods**

180 Data collection and analysis were not performed blind to the conditions of the experiments.

181 **Subjects**

182 All procedures were carried out under the auspices of a Home Office license according to the
183 Animals (Scientific Procedures) Act 1986. Nine adult male Lister Hooded rats weighing 300-
184 350g were individually housed under partial light-cycle shift (6h) to allow recordings during
185 their circadian dark cycle. They were mildly food restricted (to 90% free-feeding weight) and
186 were weighed and checked daily.

187 **Microdrives and surgery**

188 Recordings were made using tetrodes, each composed of four twisted 25 μm or eight twisted
189 17 μm polyimide-coated platinum-iridium (90%/10%) wires (California Fine Wire, CA),
190 attached to an Axona microdrive (Axona Ltd, Herts, UK). Under isoflurane anaesthesia the
191 electrodes were chronically implanted in the left or right hemisphere. For 4 rats the electrodes
192 were implanted in the RSC aimed at the granular subregion ($n = 1$ rat; co-ordinates in mm
193 from Bregma: AP: -5.5, ML: ± 0.4 , DV: 0.4), or dysgranular subregion ($n = 3$ rats; AP: -5.5,
194 ML: ± 1.0 , DV: 0.4). For three rats the electrodes were aimed at postsubiculum (AP: -7.5,
195 ML: ± 3.2 , DV: -2.0) and for two rats they were aimed at the anterodorsal thalamic nucleus
196 (ADN; AP: -1.8, ML: ± 1.4 , DV: -3.9). After the surgery, rats received meloxicam mixed with
197 condensed milk for three days for post-operative analgesia, and were given at least 7 days to
198 recover before the experiment began.

199 **Apparatus**

200 The recording apparatus (**Fig. 1a, Supplementary Fig. 1a**) was a 120 x 120 cm square box
201 with 60 cm high walls, isolated from the rest of the room by a cylindrical curtain 260 cm in
202 diameter. The box was divided into two equal rectangular sub-compartments by a 60 cm high
203 wall, in the center of which was an aperture, 10 cm at the base and 15 cm at the top, which
204 allowed free movement between compartments. The compartments were each polarized by a
205 20 cm wide x 40 cm high plastic white cue card attached to the short wall and located to the
206 left when facing the doorway. Walls and floor were covered with black vinyl sheets, allowing
207 the experimenter to wipe each compartment with a sponge moistened with lemon or vanilla
208 food flavoring so as to allow the rat to distinguish the compartments. Six circularly arranged
209 ceiling lights lighted the box and a non-tuned radio was fixed to the ceiling in a central
210 position relative to the box, producing a background noise >70 dB to mask un-controlled
211 directional sounds. For recordings made in darkness, the cue cards were removed so as to
212 minimize focal olfactory/tactile landmarks.

213 **Recording setup and procedure**

214 For recording, the microdrive connector was attached to the headstage/recording cable
215 through which the signals from each wire were amplified, filtered, digitized (48 kHz) and
216 stored by an Axona DacqUSB acquisition system. Spikes were amplified 3000-5000 times
217 and bandpass-filtered between 0.8 and 6.7 kHz; local field potential (LFP) signals were
218 amplified 1000 times and filtered between 0 and 475 Hz. Two light-emitting diodes (LEDs),
219 one large and one small and separated by 5 cm, were attached to the headstage assembly to
220 provide the position and the orientation of the rat's head. The LEDs were imaged with an
221 overhead camera at a sampling rate of 50 Hz.

222 Beginning 1 week after surgery, the animals were screened daily for single unit activity.
223 Screening were made in a small box, outside the curtain. Tetrodes were lowered 50 μm if no
224 single unit activity was found, or after a complete recording session. When a set of units was
225 isolated, the animal was transferred to the experimental apparatus inside the curtained area
226 and a sequence of five recording trials was run, as follows:

227 Trial 1 (Baseline): The orientation of the box was random with respect to the outside room.
228 Rats were placed in one of the compartments, facing in a randomly determined direction. For
229 two RSC implanted rats, starting compartments were initially the same for every trial, but
230 then switched to being randomly selected. For the remaining two RSC implanted rats it was
231 always random. For 10 minutes the animals freely moved between compartments foraging for
232 cooked sweetened rice thrown in sporadically by the experimenter.

233 Trial 2 (Rotated baseline): As for trial 1 but the box was randomly rotated by 45° or 90° or
234 180° , clockwise or counter-clockwise, to check local cue control of directional firing.

235 Trial 3 (Door closed odor 1): The apparatus was again arbitrarily rotated and the animal
236 placed in one of the compartments (randomly chosen): the connecting door was closed so the
237 rat was confined to that compartment for a five-minute trial. This was to see whether the odor
238 cues alone were enough to reinstate the correct orientation of firing.

239 Trial 4 (Door closed odor 2): The apparatus was rotated and the rat recorded in the other
240 compartment for five min.

241 Trial 5 (Baseline): A last standard 10-min door-open trial was run with the apparatus having
242 the same orientation as in trial 1.

243 Between trials, animals were removed from the apparatus and placed in a box in a random
244 location outside the curtain for 2 minutes, in order to let the experimenter manipulate the box
245 (rotation of the apparatus and/or closing or opening the door). The animal was then mildly
246 disoriented, by rotating its holding box, before the next trial.

247 For some recording sessions, two ten-minute darkness trials were added after trial 5. For the
248 first of these (trial 6 – Darkness), animals were not removed from the box after trial 5, but the
249 computer screen and ceiling lights were turned off before recording began. After this trial, the
250 animal was removed, the box randomly rotated and the rat mildly disorientated before the last
251 darkness trial (trial 7 – Rotated Darkness).

252 **Data analysis**

253 Spike sorting was performed manually using the graphical cluster-cutting software Tint
254 (Axona) with the help of an automated clustering algorithm (Klustakwik 3.0; ¹⁶). Units
255 having inter-spike intervals < 2 ms (refractory period), were removed due to poor isolation, as
256 were cells with a peak firing rate ≤ 1 Hz. In order to prevent repeated recordings of the same
257 cell over days, clusters that recurred on the same tetrodes in the same cluster space across
258 recording sessions were only analyzed on the first day.

259 The rat's head direction was calculated for each tracker sample from the projection of the
260 relative position of the two LEDs onto the horizontal plane. The directional tuning for each
261 cell was obtained by dividing the number of spikes fired when the rat faced a particular
262 direction (in bins of 6°) by the total amount of time the rat spent facing that direction. The
263 peak firing rate was defined as the rate in the bin with the highest rate; the angle of this bin is
264 the cell's preferred firing direction.

265 **Directionality analysis**

266 The Rayleigh vector was used to assess directional specificity, with significant directionality
267 being assigned to cells whose Rayleigh vector score exceeded the 99th percentile of a control
268 distribution. For the control procedure, for each cell's trial 1 data we shifted the time of every
269 spike by a uniform amount, chosen randomly from between 20 seconds and the recording
270 duration minus 20 seconds; this was repeated 400 times per cell (1090 cells x 400 = 436000
271 rotations). The 99th percentile value came to 0.26, similar to that reported in previous HD cell
272 studies^{17,18}. Thus, all cells for which the Rayleigh vector length was greater or equal to 0.26
273 and firing rate exceeded 1Hz were classified as HD cells. The cells selected for the study
274 were required to reach selection criteria in both trials 1 and 5.

275 Because of the unexpected observation of cells that fired in two opposing directions, we
276 adapted the above directionality analysis by using an angle-doubling procedure in which the
277 heading angle of each spike was multiplied by two and the results plotted modulo 360°: this
278 has the effect of converting a bi-directional distribution to a unimodal one, from which the
279 population of directionally firing neurons could be selected using the 99th percentile criterion
280 computed as before and equal to 0.22.

281 We tested whether all 360° of compass heading were represented in the directional cells we
282 recorded by referencing the firing direction of each cell to the lemon-compartment orientation
283 in trial 1. We then tested the non-uniformity of the distribution of angular distances with a
284 Rayleigh test.

285 Selection of BD cells

286 We selected BD cells by defining a “flip score” above which cells were considered bi-
287 directional, and below which they were uni-directional. Flip score was calculated with an

288 autocorrelation procedure, by rotating the polar firing rate plot in steps of 6° and calculating
289 the correlation between the rotated and unrotated plots at each step. The bi-directional pattern
290 was apparent as a sinusoidal modulation of this autocorrelation with a peak at 180°
291 (**Supplementary Fig. 4**). The flip score for each cell was defined as the difference between
292 the correlations at the expected peak (180°) and the expected troughs (90°). For the entire
293 population of directional cells this yielded two clusters (**Fig. 2** and **Supplementary Fig. 4**),
294 the local minimum between which – value 0.6 – was used to separate BD from HD cells. BD
295 cells selected for the study were those that reached vector length and flip score criteria in both
296 trials 1 and 5.

297 Cell isolation analysis

298 Cell isolation analyses were performed to rule out the hypothesis that BD cells were really
299 two co-recorded classic HD cells with opposing tuning curves.

300 (1) Cluster space analysis (**Supplementary Fig. 5a**). This analysis sought to establish
301 that the clusters from the spikes belonging to the two individual tuning curves of BD cells
302 were no further apart than the clusters of clearly uni-directional HD cells arbitrarily divided
303 in two. This was based on scatterplots of the key waveform clustering parameter, which was
304 peak-trough amplitude. For BD cells, we extracted two sub-clusters containing spikes emitted
305 in the 180-degree range surrounding each tuning curve peak, found their center of mass
306 (CoM) in the scatterplot cluster-space, and calculated the distance between the two CoMs.
307 Results were compared to a control data set comprising the spikes from HD cells that had
308 been randomly allocated to one or other of two sub-clusters; we then calculated the distance
309 between the CoMs of these. This procedure was repeated 2000 times per cell. Data from the
310 BD cells and the control data were compared with a two-sample *t*-test.

311 (2) In a second analysis (**Supplementary Fig. 5b**), we calculated the probability that
312 failure to separate the clusters of HD cells would have resulted in tuning-curve pairs that just
313 happened to be 180° apart. To do this we randomly (with replacement) selected pairs of HD
314 cells from the total pool, 10000 times, and for each pair we cross-correlated the tuning curves
315 and derived the angle of the highest correlation. Then, we calculated the percentage of cells
316 with an angular distance at $180 \pm 12^\circ$ (corresponding to two bins of 6°) and compared this,
317 using a Chi-squared test, with the observed data.

318 (3) In the last analysis, we computed the Pearson's correlation coefficient between firing
319 rates for the two tuning curves (**Supplementary Fig. 5c**) – if these were from different cells
320 then the rates should be no more correlated than those of any two randomly selected cells.
321 The correlation value was compared to control correlations generated by randomly selecting,
322 with replacement, 10 000 pairs of HD cells.

323 Directionally color-coded spatial spike maps

324 Directional color-coded spike maps were constructed in order to visually display the spatial
325 distribution of directional activity. We first defined a color map with a circular gradient of
326 color ranging in 90° bins from blue to green to red to yellow (Fig. 1b). For each cell, we
327 aligned the direction of blue in the color map with the peak firing bin in trial 1, with all other
328 directions being color accordingly, and assigned each spike the appropriate color based on its
329 associated head direction. We then generated a spatial spike plot by smoothing the path of the
330 rat in 20 ms bins and overlying it at the appropriate places with the color-coded spikes.

331 Compartmental analysis

332 Some neurons had bi-directional tuning curves even in individual sub-compartments of the
333 apparatus and so we investigated whether these behaved like HD cells that periodically
334 reversed their tuning curve direction, or more like cells with simultaneous, opposing tuning

335 curves. Analysis was performed on the two tuning curves for the whole apparatus, and also
336 for each individual compartment on the baseline trial. We identified epochs in the recording
337 trial when the rat faced continuously in the direction ($\pm 45^\circ$) of one or other tuning curve,
338 and then within these epochs we computed the firing rate (no. spikes divided by epoch
339 duration), and firing rate spread (standard deviation of firing rates across epochs).

340 Directional activity in darkness and in the open field

341 Directionally modulated cells were recorded in darkness so as to determine whether activity
342 was maintained between light and dark trials. For each cell we computed (1) the vector length
343 and the flip score as described previously, and (2) the Pearson correlation coefficient of each
344 cell's directional firing rates between continuous light-dark trials 5 and 6, and between the
345 two dark trials 6 and 7, and compared them using a Kruskal-Wallis non-parametric test.

346 Nine BD cells were additionally recorded in a 120 cm x 120 cm open-field after 5
347 experimental recording sessions. For each BD cell, we calculated the vector length and the
348 flip score to investigate whether they share directional properties found in the two
349 compartment apparatus.

350 Spatial rate maps and spatial correlation analysis

351 Spatial rate maps were generated by dividing the two-compartment apparatus into an array of
352 40 x 40 square bins, each 3 x 3 cm in size. Spikes per bin were divided by time spent in that
353 bin to provide a firing rate (Hz). Smoothed firing rate maps were then generated following
354 Spiers et al.¹⁷, by using a boxcar procedure in which the firing rate in each bin was replaced
355 by that of the mean of itself plus the immediately surrounding bins (8 for central bins, 5 for
356 edge bins and 3 for corner bins). In both raw and smoothed rate maps, pixels that were not

357 visited by the rat were displayed in white. The firing rate of the cell is color-coded from low
358 (light blue) to high (dark red).

359 To estimate the stability of the spatial activity, pixel-by-pixel cross-correlations were made
360 on the unsmoothed data from the two compartments – the first using the original maps, and
361 the second with one compartment rotated by 180°, in order to see whether spatial patterns
362 reversed in the same way that the directional patterns of BD cells did.

363 LFP/spiking characteristics and movement correlates

364 For recordings from the three brain areas we looked at spiking characteristics for the five cell
365 types (PoS HD, ADN HD, RSC HD, RSC BC-BD and RSC WC-BD) including peak firing
366 rate and inter-spike interval (ISI) histogram.

367 For the ISI analysis, a histogram of ISIs with 2ms bins was generated for each cell type and
368 the peak was taken as the center of the bin with the highest count. Inspection of the ISI
369 histograms suggested different decay times for the different cell types so we calculated decay
370 time by fitting, to the histogram, a one-term exponential decay function of the form $y =$
371 $a \cdot \exp(b \cdot x)$ from the peak to peak + 1 second, using the *fit* function from MATLAB's Curve
372 Fitting Toolbox. Time to half-peak was then taken as the time taken for the exponential fit to
373 decay to half the peak value.

374 For retrosplenial WC-BD, BC-BD, and HD cells, ISIs were also considered only for periods
375 of time where head direction was within +/- 45° of the preferred firing direction of the cell.
376 For HD cells, this was taken as the location of peak firing rate in the polar plot. For BD cells,
377 this same method was used to find one preferred firing direction, and then the other peak was
378 found using a circular autocorrelation. For the exponential curve-fitting, the lowest-spiking

379 25% of all cells were excluded (those with fewer than 145 spikes occurring within +/- 45° of
380 the peak direction for that cell).

381 **Statistics**

382 No statistical methods were used to pre-determine sample sizes but our sample sizes are
383 similar to those reported for HD cells in previous studies^{7, 9, 10}. Statistical tests included
384 Student's t-test, ANOVA, Pearson's correlation, Chi-square, Rayleigh test, Mann-Whitney U,
385 circular V-test. Data distribution was assumed to be normal but this was not formally tested.

386 **Histology**

387 At the completion of the experiment, rats received an overdose of pentobarbital and were
388 perfused intracardially with 0.9% saline followed by 4% formaldehyde. The brains were
389 removed, stored 1 day in formaldehyde, followed by 30% sucrose solution, and finally frozen
390 with dry ice. 30- µm-thick coronal sections for ADN and RSC animals and sagittal sections
391 for PoS animals were mounted on glass slides and stained with cresyl violet or thionine. The
392 position of the tips of the electrodes were determined from digital pictures, acquired with an
393 Olympus microscope (Olympus Keymed, Southend-on-Sea, U.K.) and imported into an
394 image manipulation program (Gimp 2.8, distributed under General Public License).
395 Recording sites were determined by measuring backwards from the deepest point of the track,
396 and identifying with the help of the rat brain atlas from Paxinos and Watson¹⁹.

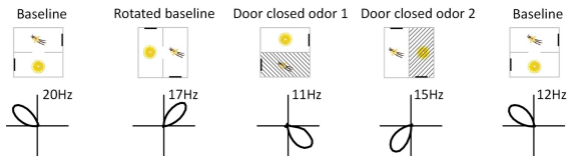
397 **Data and code availability**

398 The raw and analyzed data and code that support the findings of this study are available from
399 <https://discover.ukdataservice.ac.uk/series/>

400 **Methods references**

- 401 16. Kadir, S.N., Goodman, D.F.M. & Harris, K.D. *Neural Comput.* **26**, 2379–94 (2014).
- 402 17. Bonnevie, T. et al. *Nat. Neurosci.* **16**, 309–17 (2013).
- 403 18. Giocomo, L.M. et al. *Curr. Biol.* **24**, 252–262 (2014).
- 404 19. Jeewajee, A., Barry, C., O’Keefe, J. & Burgess, N. *Hippocampus* **18**, 1175–1185
405 (2008).
- 406 20. Paxinos, G. & Watson, C. *Elsevier Acad. Press* **170**, 547–612 (2007).

a Head direction (HD) cell



b Bi-directional (BD) cell

